Supplemental Document

Optics EXPRESS

TDI-like multi-slit hyperspectral imaging for enhanced throughput via the Kalman filter: supplement

YAOYAO HU,[1,2] CHENGWEN LIU,[1] ZI HENG LIM,[1] YI QI,[1,3] HAOYANG SUN,[1] JUN CHANG,[2] AND GUANGYA ZHOU[1,*]

[1] *Department of Mechanical Engineering, National University of Singapore, 9 Engineering Drive 1, 117575, Singapore*
[2] *School of Optics and Photonics, Beijing Institute of Technology, 100081 Beijing, China*
[3] *Institute of Bioengineering and Bioimaging, Agency for Science, Technology and Research (A*STAR), 11 Biopolis Way, Helios, #02-02, 138667, Singapore*
[*] *mpezgy@nus.edu.sg*

Supplement DOI: https://doi.org/10.6084/m9.figshare.22313557

Parent Article DOI: https://doi.org/10.1364/OE.484016

TDI-like multi-slit hyperspectral imaging for enhanced throughput via Kalman filter: supplemental document

1. Encoding on multi-slit

The KF algorithm described in the main paper is used in the theoretical simulation of our dynamic model. In the theoretical simulation, the measurement noise added is twice as large as the real signal. The reconstruction is performed using KF with a recurrence number of 200. The results of the dynamic model in which the measurement matrix is encoded are illustrated in Fig. S1**a**, which demonstrates that the estimated signal and the real signal converges after recurrence to the 50th time step. The results in Fig. S1**b** indicate that a measurement matrix that is not encoded leads to very unsatisfactory noise reduction capability. Therefore, we conclude that the multi-slit needs to be encoded in the MSHSI setup, but the method of encoding should be determined experimentally as it involves the measurement noise in the actual setup.

In the actual setup, some slits of the multi-slit are closed on the DMD because of the encoding pattern, which means light from these closed slits do not enter the CCD. Thus, measurement matrix $\mathbf{H}_k$ is obtained by selecting different slit encoding patterns a_i (i = 1, 2, …, M) in Eq. (3) to investigate their HSI performance.

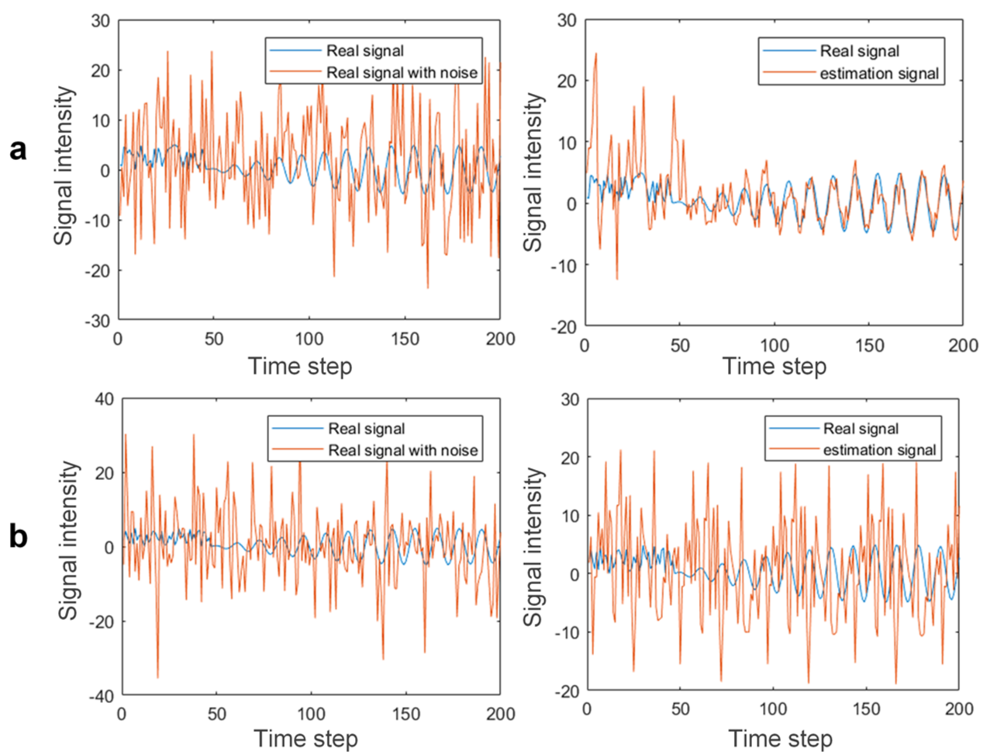

Fig. S1 Results of simulation in a dynamic model. **a** Measurement matrix with Hadamard code. **b** Measurement matrix without any code.

2. Determination of Q and R-value

Our system acquired measurement data in FE mode. In the reconstruction algorithm, Q is kept constant at 0.15 and R is set at 0.0001, 0.01, 0.25, 1, 4, and 9. The reconstruction results are shown in Fig. S2. Decreasing R improves the imaging quality and is relatively consistent when R≤1. Therefore, R=1 is used in our subsequent experiments.

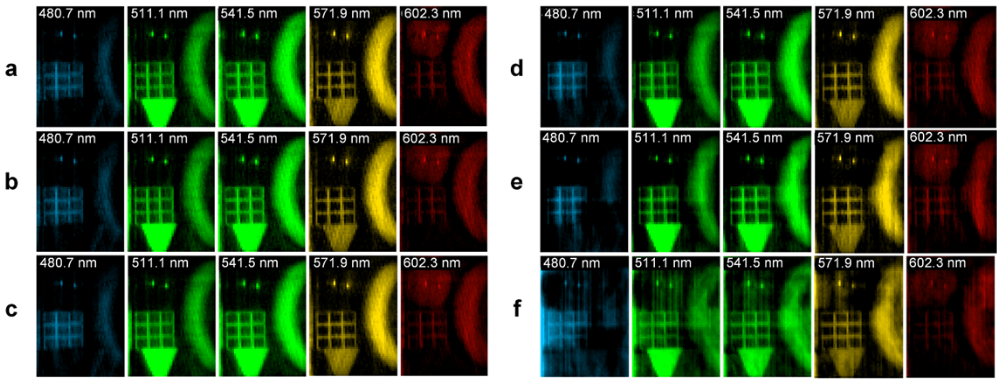

Fig. S2 Reconstructed images with **a** R=0.0001, **b** R=0.01, **c** R=0.25, **d** R=1, **e** R=4, **f** R=9.

Similarly, we did another set of reconstruction where R is kept constant at 1 and Q is set at 1, 0.5, 0.2, 0.15, 0.1, 0.01, 0.001 and 0.0001. The reconstruction results are shown in Fig. S3. Increasing Q improves the spatial resolution and the imaging quality tends to be consistent when Q≥0.1. Therefore, Q=0.15 is used in our subsequent experiments.

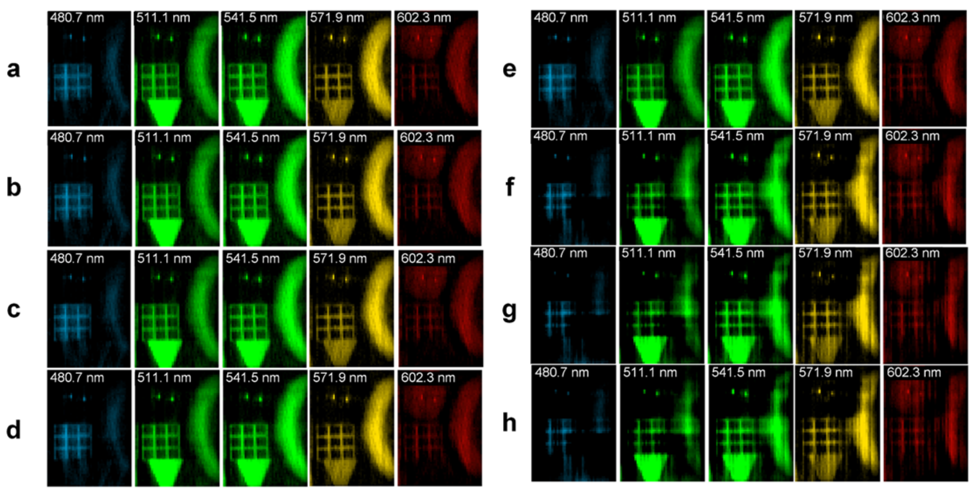

Fig. S3 Reconstructed images with **a** Q=1, **b** Q=0.5, **c** Q=0.2, **d** Q=0.15, **e** Q=0.1, **f** Q=0.01, **g** Q=0.001, **h** Q=0.0001.

3. Comparison of encoding modes

In our proposed KF-based MSHSI system, the initial values in the state vector before the first pushbroom scan and measurement are set to zero. In fact, the scenes other than the TOI will necessarily focus on the CCD as measurements before the first pushbroom scan (the initial zero state vector value is not zero). Therefore, we investigate a third encoding mode called semi-dynamic encoding (SDE) mode. The SDE mode masks the scenes other than the TOI by encoding the multi-slit. The SDE mode use the same encoding weight a_i (i = 1, 2, …, M) in Eq. (3), but the number of slits increases one by one from M=1 to M=47, forming 47 encoding patterns with different number of slits. When k>47, the DMD retains the 47th encoding pattern.

The MSHSI acquires data of the same scene in different encoding modes at a distance of 2.7 m under a 70 W sunlight LED illumination environment. These encoding modes are FE, SDE and DE modes each paired with Hadamard code and FE, SDE and DE modes each paired with random code. The reconstruction parameters are kept as Q=0.15 and R=1. The results are presented in Fig. S4. The reconstruction using FE and SDE modes with Hadamard code have properly restored the objects in the scene, while reconstruction with the other encoding modes is much noisier. Fig. S4**a-b** and Fig. S5 justify that the initial zero state vector value has no impact on the output after some pushbroom steps.

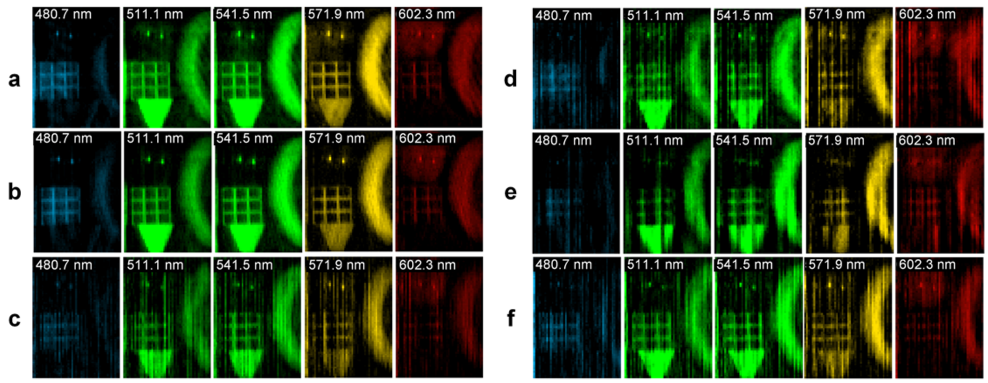

Fig. S4 Images of the TOI sliced at different wavelengths of the reconstructed data cube when the MSHSI is operated in **a** FE with Hadamard code, **b** SDE with Hadamard code, **c** DE with Hadamard code, **d** FE with random code, **e** SDE with random code, **f** DE with random code.

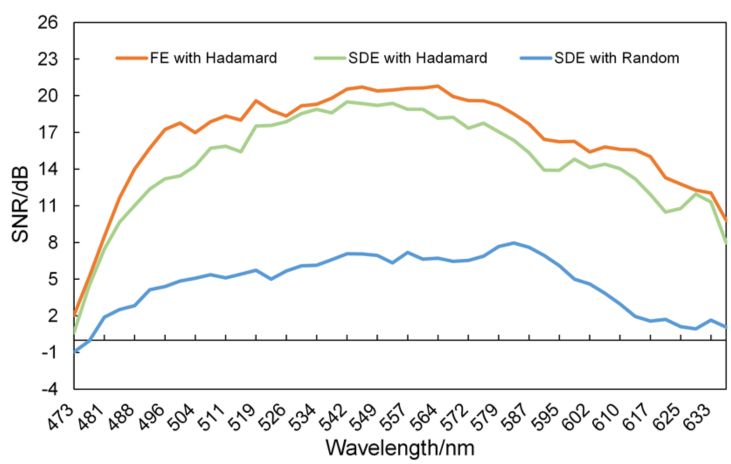

Fig. S5 SNR of the MSHSI working in FE and SDE modes.

4. Reconstruction of different scenes

Fig. S6 shows the scene we put together in the lab to evaluate the performance of the MSHSI, captured by a cell phone camera. The MSHSI acquires the measurement data in a pushbroom process using FE with Hadamard code. The pushbroom direction is from left to right as depicted by the arrow in Fig. S6. The measurement data of the three TOIs in the red, green, and yellow boxes are separately processed by KF and their reconstructed results are presented in Fig. S7, Fig. S8, and Fig. S9, respectively, demonstrating that the reconstruction of different TOIs are not affected by the nearby scenes.

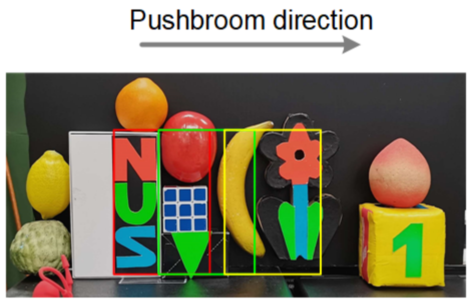

Fig. S6 Test scene captured by a cell phone camera.

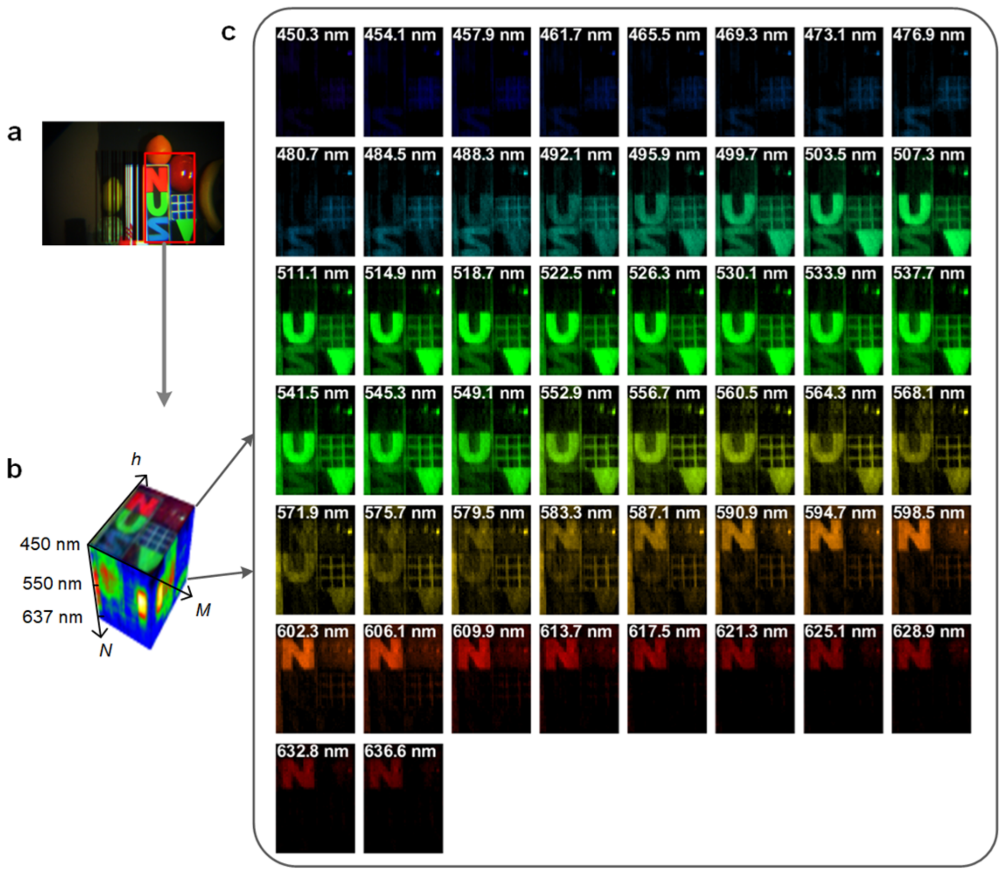

Fig. S7 Reconstruction results of the TOI in the red box. **a** Image on the CMOS in the auxiliary imaging system. **b** Reconstructed spatio-spectral data cubes for the TOI. **c** Images of the TOI sliced at 50 different wavelengths from the reconstructed data cube.

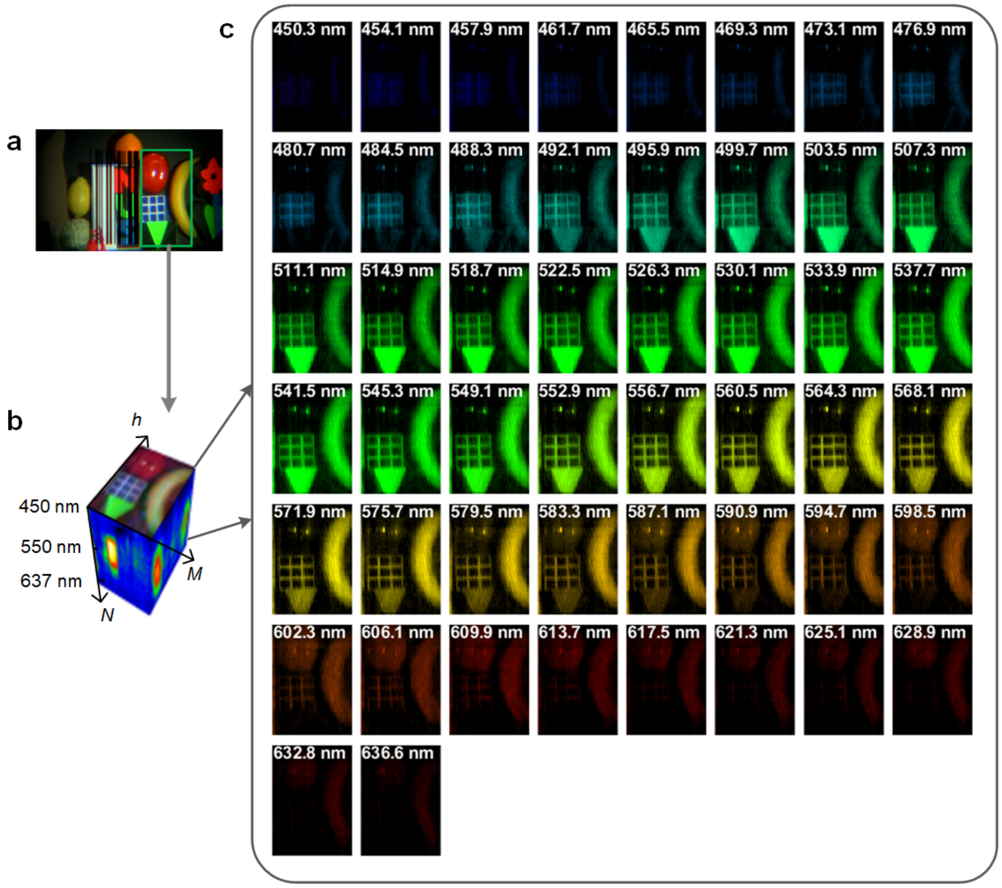

Fig. S8 Reconstruction results of the TOI in the green box. **a** Image on the CMOS in the auxiliary imaging system. **b** Reconstructed spatio-spectral data cubes for the TOI. **c** Images of the TOI sliced at 50 different wavelengths from the reconstructed data cube.

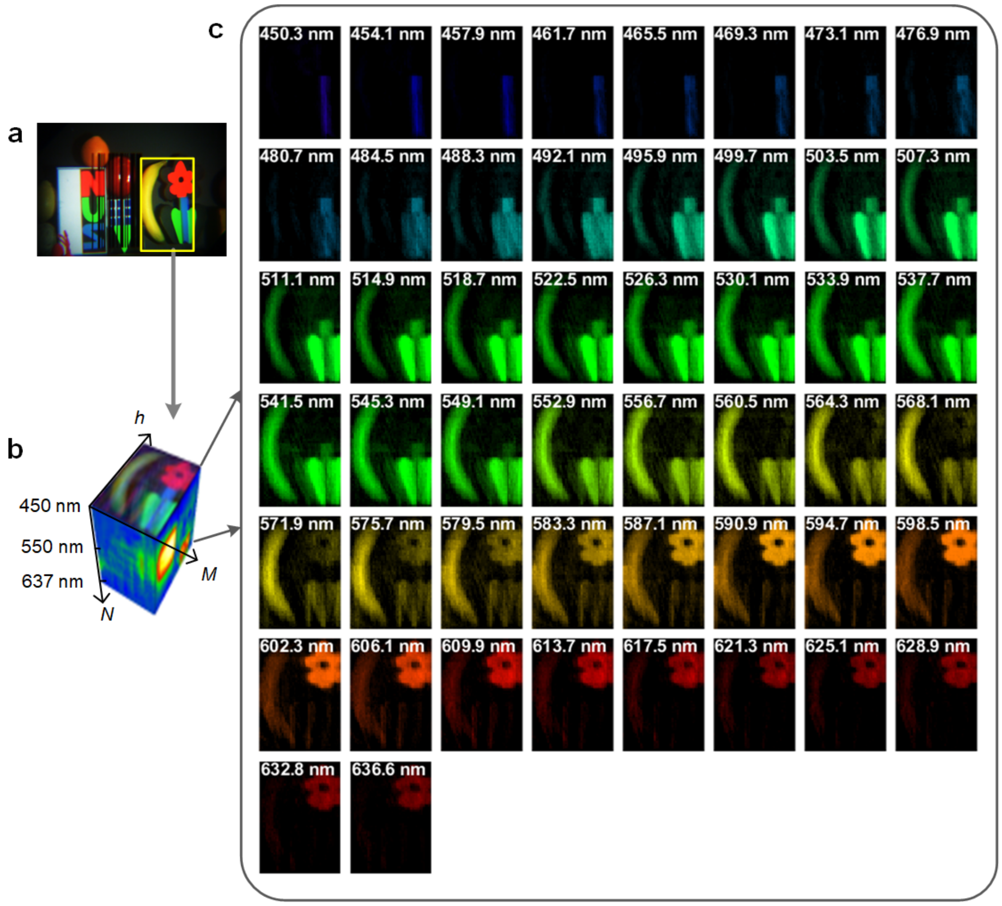

Fig. S9 Reconstruction results of the TOI in the yellow box. **a** Image on the CMOS in the auxiliary imaging system. **b** Reconstructed spatio-spectral data cubes for the TOI. **c** Images of the TOI sliced at 50 different wavelengths from the reconstructed data cube.

5. Reconstruction and acquisition time

The reconstruction takes roughly 2 minutes, but the reconstruction speed can be improved if the GPU is configured to calculate in parallel. The acquisition time for our prototype is currently around 94 seconds; this is because our proof-of-concept system scans in a quasi-static pushbroom fashion, whereby the rotation mirror rotates to a position and stops to acquire an image before rotating to the next step and repeating the acquisition. The acquisition time can be significantly improved in an actual dynamic pushbroom process where the CCD image acquisition is synchronized and triggered by a continuous pushbroom scan motion.

6. CCD information

As shown in the Fig. S10, the CCD has 3840×2160 pixels (black box in the figure). The red dashed box and the green box indicates the area on the CCD used to capture the hyperspectral images when in single slit mode and multi-slit mode, respectively.

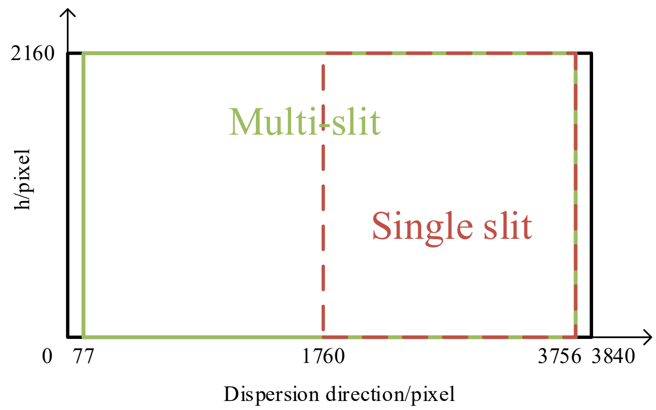

Fig. S10 Effective part of CCD used in single-slit mode (red dashed box) and multi-slit (green box) mode. Black box indicates the full CCD active area.